Supporting Material

Auditory hair cell centrioles undergo confined Brownian motion throughout the developmental migration of the kinocilium

Léa Lepelletier, Jacques Boutet de Monvel, Johanna Buisson, Chantal Desdouets, and Christine Petit

Supporting Figures

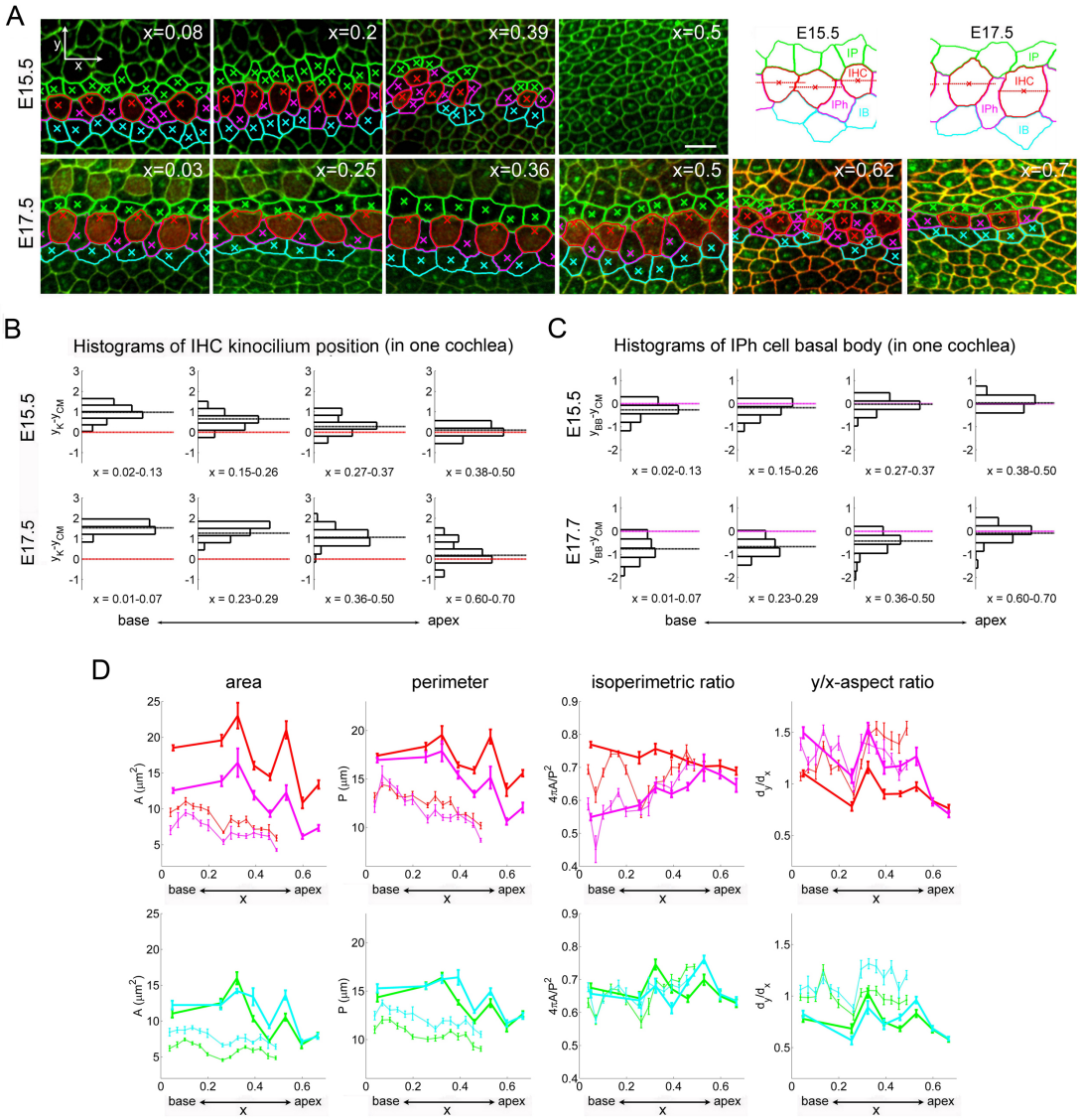

Figure S1. (A) Series of surface confocal images of the organ of Corti at various positions along cochleas microdissected at E15.5 and E17.5, and immunolabelled to reveal the centrioles (green), the apical cell-cell junctions (green also), and the hair cells (red) (cf. Methods). Basal body positions (crosses) and watershed contours of IHCs and of supporting cells contacting IHCs are overlaid. Scalebar : 5 µm. Supporting cells were classified into : inner pillar cells (IP, green), inner phalangeal cells (IPh, magenta), or inner border cells (IB, cyan), according as their contours lay above all adjacent IHCs, intersected one of them, or lay below all of them (see upper-right inset). (B,C) Histograms of the radial coordinate $y_{\mathrm{BB}} - y_{\mathrm{CM}}$ of basal body position relative to CM (colored dashed line) in individual IHCs (B) and in individual IPh cells (C). Data for one cochlea at each stage. Black dashed lines show the histograms' medians. (D) Geometric characteristics of IHCs and adjacent supporting cells as a function of x. From left to right : apical surface area, perimeter, isoperimetric ratio ($4\pi \times$ area/perimeter^2), and y/x-aspect ratio. Upper graphs, IHCs (red) and IPh cells (magenta) ; lower graphs, inner pillar cells (green) and inner border cells (cyan).

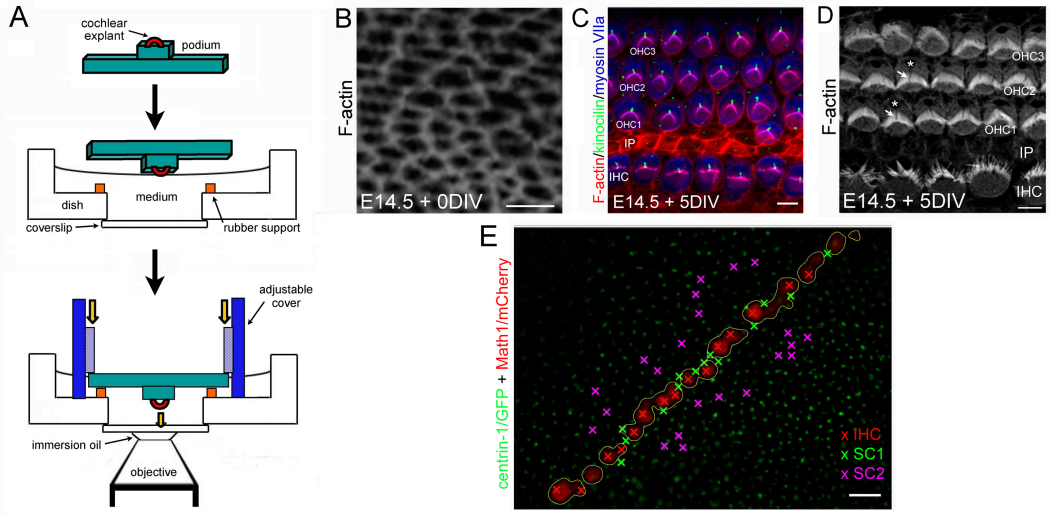

Figure S2. Tracking hair cell centriole movements by videomicroscopy. (A) Experimental setup. Top : The matrigel-coated custom podium on which cochlear explants were let to adhere. Middle : The podium is turned upside down, placed onto two rubber pieces fixed at the bottom of a culture dish, and left to relax in medium for $>$ 5 hours at 37°C. Bottom : An adjustable plexiglass cover allows the podium boundaries to be pressed against the rubber pieces to set the explant's surface in position on the microscope's stage. (B-C) Surface views of cochleas immunostained to reveal actin filaments, kinocilium axonema, and hair cell cytoplasm, and imaged by confocal microscopy (see Methods). (B) Cochlea isolated at E14.5 and immunostained for F-actin on the same day. (C,D) Cochleas isolated at E14.5 and immunostained after 5 days of culture. (C) F-actin (red), kinocilium axonema (green) and hair cell cytoplasm (blue). (D) F-actin only. Image in (D) was deconvolved using the Huygens software. The cytoplasmic channel of the cuticular plate (asterisk) and the kinocilium (arrow) are seen by their absence of F-actin staining. (E) Videomicroscopy image of the surface of a Centrin-1/GFP-Math1/mCherry mouse cochlear explant at E14.5. Crosses indicate cells whose centrioles were selected for analysis. IHC, mCherry-stained inner hair cells (delineated by yelow contours) ; SC1, supporting cells adjacent to an IHC ; SC2, other supporting cells. Scale bars : 5 µm.

IHC	stage 1	stage 2	stage 3
1-center trajectories	$n = 28$	$n = 117$	$n = 52$
rms step size, $\langle\|\delta x(t)\|^2\rangle^{1/2}$	53.5 ± 4.2	77.4 ± 3.2	78.2 ± 4.8
$MSD(t = 2s)$	3.43 ± 0.56	7.12 ± 0.59	7.23 ± 0.88
	$\times 10^{-3}$	$\times 10^{-3}$	$\times 10^{-3}$
MSD fit - confinement area, A	3.41 ± 0.84	7.07 ± 1.17	7.77 ± 1.29
	$\times 10^{-3}$	$\times 10^{-3}$	$\times 10^{-3}$
MSD fit - relaxation time,τ_0	0.57 ± 0.35	0.73 ± 0.31	0.77 ± 0.40
MSD fit - random drift coef.,D_0	0.27 ± 0.15	0.72 ± 0.25	0.35 ± 0.09
	$\times 10^{-4}$	$\times 10^{-4}$	$\times 10^{-4}$
MSD fit - directed drift coef.,u_0	4.34 ± 0.29	4.69 ± 0.43	2.52 ± 0.21
cochlear extension velocity, u_{CE}	4.43 ± 0.67	4.44 ± 0.60	3.50 ± 0.47
confinement force	0.10 ± 0.01	0.11 ± 0.01	0.11 ± 0.01
2-center trajectories	$n = 5$	$n = 34$	$n = 14$
$MSD_1(t = 2s)$	9.9 ± 4.7	11.6 ± 2.0	10.6 ± 2.0
	$\times 10^{-3}$	$\times 10^{-3}$	$\times 10^{-3}$
$MSD_2(t = 2s)$	15.9 ± 8.3	27.8 ± 4.5	22.3 ± 5.5
	$\times 10^{-3}$	$\times 10^{-3}$	$\times 10^{-3}$
$\Delta(t = 10s)$	20.0 ± 10.0	30.9 ± 4.7	23.3 ± 5.0
	$\times 10^{-3}$	$\times 10^{-3}$	$\times 10^{-3}$
$\delta_1 = 2\sqrt{MSD_1(t = 2s)}$	0.18±0.04	0.19±0.02	0.19±0.02
$\delta_2 = 2\sqrt{MSD_2(t = 2s)}$	0.21±0.05	0.30±0.03	0.27±0.04
intercentriole distance, $\overline{r(t)}$	445 ± 24	451 ± 15	430 ± 29
std of $r(t)$, σ_r	61.2 ± 9.0	78.4 ± 5.2	84.4 ± 8.3
rms distance steps, $(\overline{\delta r(t)^2})^{1/2}$	68.7 ± 13.7	86.4 ± 6.0	87.6 ± 10.1
intercentriole angle std,σ_θ	11.1 ± 2.6	17.3 ± 1.8	17.0 ± 3.1
rms angle steps, $(\overline{\delta\theta(t)^2})^{1/2}$	12.6 ± 3.1	16.8 ± 1.7	16.8 ± 3.4

Table S1. Averaged characteristics of IHC centriole trajectories. Values (mean ± standard error) are given for the three age groups (stages 1, 2, and 3) defined in the text. MSD fit parameters correspond to the best fit of Eq. 3 in the text to the averaged MSD curve obtained at the given stage ; standard errors on these parameters were estimated by the bootstrap method. Units : distances in nm ; areas and MSD in μm^2 ; velocities in nm/s ; forces in pN ; angles in degrees.

	SC1			SC2		
	stage 1	stage 2	stage 3	stage 1	stage 2	stage 3
1-center trajectories	$n = 30$	$n = 87$	$n = 87$	$n = 69$	$n = 204$	$n = 211$
rms step size, $\langle\|\delta x(t)\|^2\rangle^{1/2}$	47.1 ± 3.0	69.9 ± 3.5	69.2 ± 4.0	43.0 ± 2.2	52.5 ± 1.7	56.6 ± 1.6
$MSD(t = 2s)$	2.54 ± 0.32 $\times 10^{-3}$	5.91 ± 0.56 $\times 10^{-3}$	6.12 ± 0.71 $\times 10^{-3}$	2.23 ± 0.23 $\times 10^{-3}$	3.35 ± 0.23 $\times 10^{-3}$	3.71 ± 0.22 $\times 10^{-3}$
MSD fit - confinement area, A	2.71 ± 2.88 $\times 10^{-3}$	6.09 ± 0.87 $\times 10^{-3}$	6.84 ± 0.94 $\times 10^{-3}$	2.02 ± 0.46 $\times 10^{-3}$	3.09 ± 0.71 $\times 10^{-3}$	3.20 ± 0.30 $\times 10^{-3}$
MSD fit - relaxation time, τ_0	1.21 ± 0.68	0.78 ± 0.31	0.92 ± 0.42	0.59 ± 0.46	0.55 ± 0.34	0.38 ± 0.23
MSD fit - random drift coef., D_0	0.35 ± 0.30 $\times 10^{-4}$	0.44 ± 0.12 $\times 10^{-4}$	0.41 ± 0.09 $\times 10^{-4}$	0.44 ± 0.09 $\times 10^{-4}$	0.55 ± 0.11 $\times 10^{-4}$	0.66 ± 0.07 $\times 10^{-4}$
MSD fit - directed drift coef., u_0	4.37 ± 0.33	5.02 ± 0.54	2.14 ± 0.22	4.37 ± 0.27	5.46 ± 0.38	2.30 ± 0.15
confinement force	0.11 ± 0.01	0.13 ± 0.01	0.12 ± 0.01	0.10 ± 0.01	0.12 ± 0.01	0.10 ± 0.01
2-center trajectories	$n = 8$	$n = 30$	$n = 48$	$n = 19$	$n = 86$	$n = 86$
$MSD_1(t = 2s)$	4.9 ± 1.0 $\times 10^{-3}$	14.8 ± 3.4 $\times 10^{-3}$	11.6 ± 1.8 $\times 10^{-3}$	3.3 ± 0.5 $\times 10^{-3}$	6.5 ± 0.8 $\times 10^{-3}$	9.5 ± 0.9 $\times 10^{-3}$
$MSD_2(t = 2s)$	12.6 ± 2.2 $\times 10^{-3}$	30.3 ± 4.4 $\times 10^{-3}$	22.5 ± 3.0 $\times 10^{-3}$	7.0 ± 1.0 $\times 10^{-3}$	19.5 ± 1.9 $\times 10^{-3}$	18.4 ± 1.7 $\times 10^{-3}$
$\Delta(t = 10s)$	11.4 ± 1.6 $\times 10^{-3}$	30.2 ± 5.8 $\times 10^{-3}$	23.7 ± 3.0 $\times 10^{-3}$	8.3 ± 1.2 $\times 10^{-3}$	19.2 ± 1.8 $\times 10^{-3}$	19.3 ± 1.7 $\times 10^{-3}$
$\delta_1 = 2\sqrt{MSD_1(t = 2s)}$	0.13 ± 0.01	0.21 ± 0.02	0.20 ± 0.02	0.11 ± 0.01	0.14 ± 0.01	0.18 ± 0.01
$\delta_2 = 2\sqrt{MSD_2(t = 2s)}$	0.21 ± 0.02	0.32 ± 0.02	0.27 ± 0.02	0.16 ± 0.01	0.25 ± 0.01	0.25 ± 0.01
intercentriole distance, $\overline{r(t)}$	418 ± 27	409 ± 21	429 ± 14	365 ± 28	404 ± 12	424 ± 10
std of $r(t)$, σ_r	59.4 ± 4.6	83.5 ± 6.1	70.1 ± 4.0	56.5 ± 5.6	74.2 ± 3.7	76.2 ± 2.8
rms distance steps, $(\overline{\delta r(t)^2})^{1/2}$	66.3 ± 5.6	86.7 ± 6.7	78.8 ± 4.9	49.9 ± 4.1	72.3 ± 3.5	68.6 ± 3.2
intercentriole angle std,σ_θ	9.8 ± 1.0	16.8 ± 1.6	15.3 ± 1.0	14.6 ± 2.4	15.6 ± 1.0	17.2 ± 0.8
rms angle steps, $(\overline{\delta\theta(t)^2})^{1/2}$	11.1 ± 1.3	18.1 ± 2.2	15.7 ± 1.2	12.5 ± 2.4	14.6 ± 1.1	13.0 ± 0.8

Table S2. Averaged characteristics of centriole trajectories in supporting cells. Values (mean ± standard error) are given for the three age groups (stages 1, 2, and 3) as in Table SI.

Supporting Information

S1. Centriole motion tracking algorithm

Pre-filtering step. Each image $I(x,t)$ of a given time-lapse series was first subject to a wavelet denoising algorithm as described (1). Background subtraction was then applied by taking the difference between the denoised image and a blurred version of it obtained by convolution with a "large" gaussian kernel. The full-width-at-half-maximum (FWHM) of this gaussian filter was set to $\approx 2.7\mu$m (corresponding to a standard deviation of 16 pixels). This size was large compared to the typical diffraction-limited size of GFP-centriole spots (FWHM of $0.7 \pm 0.1\mu$m, mean $\pm$ standard deviation), while being smaller than the typical cell-size (3-10μm) setting the length scale of background variations in the images.

Selection of centriole pairs. The pre-filtered GFP-images typically contained a set of well-separated pairs of diffraction-limited spots in a dark background, whose relative positions varied usually little over a duration of 10-15 min. These pairs corresponded to the images of the mother (basal body) and daughter centrioles of cochlear cells seen in the focal plane. Centriole pairs of interest were manually selected in the first image frame, and were classified in three groups according to cell-type (HC, hair cells ; SC1, supporting cells adjacent to hair cells ; SC2 other supporting cells, cf. Fig. 3A). The coordinates $c_1, \ldots, c_k$ of the reference centers of each group served as seeds to initialize the subsequent tracking step.

Tracking step. For each selected center c_i, a local search for the corresponding nearby centriole pair was performed by applying a bimodal gaussian spot detection algorithm within a small square frame initially centered on c_i. The tracking square (22 pixels accross) was adjusted at each time step so that it remained at all time centered on a unique centriole pair. The content of the tracking square could at all times be approximated by a superposition of two gaussian spots representing the diffraction-limited image of the tracked pair. The parameters of these spots (center coordinates, standard deviation radius, and center intensity) were estimated by a full least-squares fit of the parameters of either a bimodal gaussian mixture ("two-center tracking"), or a single gaussian ("one-center tracking"), against the pixel values in the tracking square. In the case of the two-center tracking, individual centriole trajectories were reconstructed using the best least-squares matching between the pairs of fitted gaussian spots at successive time steps.

S2. Analysis of centriole trajectories

We analyzed two types of hair cell centriole trajectory characteristics : *One-center trajectory quantities* characterize the trajectory of the center $\mathbf{x}(t)$ of the gaussian best-fitted to the mother/daughter centriole pair. We let $\mathbf{x}_n = \mathbf{x}(n\delta t)$ be that position after n time steps, and $\delta\mathbf{x}_n = \mathbf{x}_{n+1} - \mathbf{x}_n$ be the step vector between time steps n and $n+1$.

The one-center mean-squared displacement (MSD) of the centriole pair after a time t, defined by $MSD(t) = \langle|\mathbf{x}(t) - \mathbf{x}(0)|^2\rangle$, was estimated for a trajectory of N recorded steps from its empirical value for an n-step interval :

$$MSD_n \;=\; \frac{1}{N-n}\sum_{l=1}^{N-n} |\mathbf{x}_{l+n} - \mathbf{x}_l|^2 \approx MSD(n\delta t). \qquad (1)$$

From it we get the effective diffusion coefficient $D_{\text{eff}}(t) = MSD(t)/4t$ of the centriole pair. For unconstrained Brownian motion the MSD grows linearly with time, $MSD(t) \propto 4Dt$,

where D is the particle's free diffusion coefficient. For directed motion the MSD grows quadratically, $MSD(t) \propto u_0^2 t^2$, u_0 being the drift velocity. For a confined Brownian motion the MSD saturates to a finite value proportional to the effective area of the region in which the particle is confined (see section SI1 below).

To estimate the forces responsible for the confinement of a particular trajectory or an ensemble of trajectories, we estimated a corresponding effective confinement potential energy (2). In brief, the force maintaining the centriole pair close to its equilibrium position is assumed to be the gradient of an effective radial potential $V_{\text{conf}}(r)$ (r being the distance from the centrosome's position to the center of the potential taken as origin). If the centrioles are in thermal equilibrium over the duration of the experiments, the probability density of finding the centrosome at a distance r of the center is predicted to be Boltzmann's distribution

$$\rho_{\text{conf}}(r) = Cr \exp(-V_{\text{conf}}(r)/k_B T) \tag{2}$$

where k_B denotes Boltzmann's constant ($k_B = 1.38 \times 10^{-23}\text{J.K}^{-1}$), T is the temperature in Kelvin (set to 310 K for all experiments), and C is a normalization constant. Given an ensemble of pooled trajectories, the radial density function $\rho_{\text{conf}}(r)$ was estimated by fitting Eq. 2 to the histogram of the radial distances $r(t) = |x(t) - \langle x(t) \rangle|$ formed over time and over all trajectories of the ensemble, where $\langle x(t) \rangle$ denotes the mean-position of a given trajectory $x(t)$ after correction for the cochlear tissue drift has been applied. We adopted a power-law form for the confinement potential, $V_{\text{conf}}(r) = V_0 r^a$, where V_0 and a are referred to as the potential amplitude and exponent, respectively. The normalization constant in Eq. 2 is then given by $C = a V_0^{2/a}/\Gamma(2/a)$ where Γ is the Gamma function.

Two-center trajectory quantities characterize the relative position of the mother and daughter centrioles of a given IHC. We denote by $x_1(t)$ and $x_2(t)$ the positions of the pair of centrioles detected at time t by a bimodal gaussian fit, and $MSD_1(t)$ and $MSD_2(t)$ their respective mean-squared displacements, estimated using Eq. 1. Assuming the centriole of higher mobility to be the daughter centriole (23), we chose labels 1 and 2 so that $MSD_1(t) < MSD_2(t)$ at short times, and call centrioles 1 and 2 the putative mother and daughter centrioles, respectively. We let $z(t) = x_2(t) - x_1(t)$ be the relative position vector of the two centrioles; $r(t) = |z(t)|$ the distance separating them; and, $\theta(t)$ the polarisation angle of the centriole pair, i.e. the angle made by the vector $z(t)$ with the radial (or neural-abneural) cochlear axis at the position of measurement. We denote by z_n, r_n, θ_n, the respective values of $z(t)$, $r(t)$, and $\theta(t)$ at time $t = n\delta t$. The mean-squared displacement $\Delta(t) = \langle |z(t) - z(0)|^2 \rangle$ of the relative position vector $z(t)$ after t seconds was estimated by

$$\Delta_n = \frac{1}{N-n} \sum_{l=1}^{N-n} |\mathbf{z}_{l+n} - \mathbf{z}_l|^2 \approx \Delta(n\delta t), \tag{3}$$

and the corresponding effective diffusion coefficient by $D_{\text{eff},z}(t) = \Delta(t)/4t$. The mean, standard deviation, and root-mean-square step of the intercentriole distance were estimated by

$$\bar{r} = \frac{1}{N}\sum_{l=1}^{N} r_l; \quad \sigma_r^2 = \frac{1}{N}\sum_{l=1}^{N}(r_l - \bar{r})^2; \quad \overline{\delta r^2} = \frac{1}{N}\sum_{l=1}^{N} \delta r_l^2; \quad \delta r_l = r_{l+1} - r_l; \tag{4}$$

the mean and standard deviation of the angle $\theta(t)$, by

$$\bar{\theta} = \frac{1}{N}\sum_{l=1}^{N} \theta_l; \quad \sigma_\theta^2 = \frac{1}{N}\sum_{l=1}^{N}(\theta_l - \bar{\theta})^2; \quad \overline{\delta\theta^2} = \frac{1}{N}\sum_{l=1}^{N} \delta\theta_l^2; \quad \delta\theta_l = \theta_{l+1} - \theta_l. \tag{5}$$

S3. One-center tracking versus CM tracking of a pair of gaussian spots

We compare here the position of the gaussian spot best fitted to a given pair of gaussian spots (referred to as its "one-center" position), to the center of mass (CM) of the pair. We shall show that in the conditions of our experiments, these two positions remained close to each other. The one-center position thus provides a useful substitute to the true CM, which is in practice easier to estimate.

Thus, let us consider a pair gaussian spots in the plane, of respective positions c_1, c_2, standard deviations σ_1, σ_2, and intensities a_1, a_2 such that $a_1 + a_2 = 1$. The image formed by these two spots is the bimodal gaussian mixture

$$g_m(x) = a_1 g_{\sigma_1}(x - c_1) + a_2 g_{\sigma_2}(x - c_2) = \frac{a_1}{2\pi\sigma_1^2} e^{-\frac{(x-c_1)^2}{2\sigma_1^2}} + \frac{a_2}{2\pi\sigma_2^2} e^{-\frac{(x-c_2)^2}{2\sigma_2^2}}$$

whose CM position is given by $c_{CM} = a_1 c_1 + a_2 c_2$. We want to fit a single gaussian spot to g_m, i.e. to find a gaussian distribution $g(x) = a g_\sigma(x - c) = \frac{a}{2\pi\sigma^2} e^{-\frac{(x-c)^2}{2\sigma^2}}$ such that the mean-squared distance

$$E(c, \sigma, a) = \| g_m - g \|^2 = \int_{\mathbf{R}^2} |g_m(x) - g(x)|^2 dx$$

is minimal. The function $E(c, \sigma, a)$ can be computed using standard gaussian integral formulae :

$$E(c, \sigma, a) = \| g_m \|^2 + \frac{a^2}{4\pi\sigma^2} - 2a(a_1\lambda_1 + a_2\lambda_2)$$

where $\lambda_i = \frac{1}{2\pi(\sigma^2+\sigma_i^2)} e^{-\frac{(c-c_i)^2}{2(\sigma^2+\sigma_i^2)}}$, $i = 1, 2$. The minimum of $E(c, \sigma, a)$ is found by solving the equations $\frac{\partial E}{\partial a} = 0$, $\frac{\partial E}{\partial c} = 0$, $\frac{\partial E}{\partial \sigma} = 0$. The equation $\frac{\partial E}{\partial a} = 0$ gives the constraint $\frac{a}{4\pi\sigma^2} = a_1\lambda_1 + a_2\lambda_2$. The equation for c (which is in reality two equations, one for each component of c) is easily seen to give $(c - c_1)a_1\lambda_1 + (c - c_2)a_2\lambda_2 = 0$, which is solved by $c = \frac{a_1\lambda_1 c_1 + a_2\lambda_2 c_2}{a_1\lambda_1 + a_2\lambda_2}$. Thus, like c_{CM}, the center of the optimal spot lies on the segment joining c_1 and c_2. The equation $\frac{\partial E}{\partial \sigma} = 0$ gives a constraint on σ which we will not bother to write down explicitely. The precise location of this center can be obtained by solving the above system of equations numerically. The result is illustrated in Fig. S3 below, in which the difference $c - c_{CM}$ between the one-center position and the CM position along the segment $[c_1, c_2]$ is plotted as a function of $a_2 = 1 - a_1 \in [0, 1]$, for different values of $\sigma_1 \approx \sigma_2$, assuming unit distance between the centers ($|c_1 - c_2| = 1$). In the typical conditions of our experiments, the distance $|c - c_{CM}|$ had a mean of $\sim 5\%$ of the intercentriole distance and did not exceed 25 % (with a standard deviation $< 10\%$) of that distance.

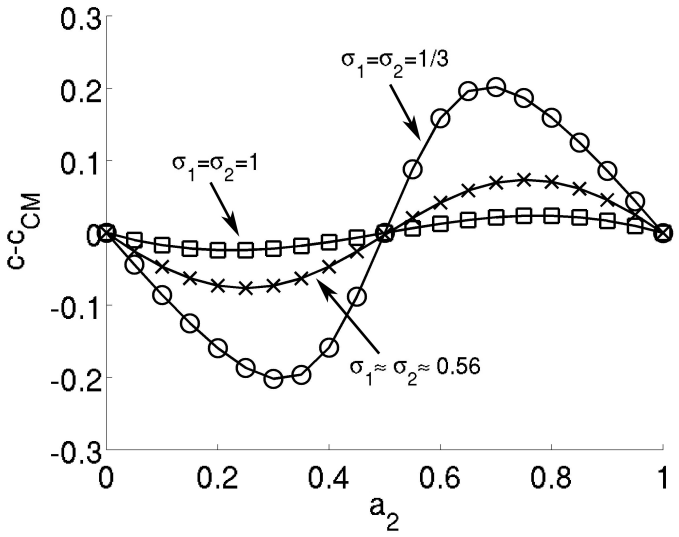

Figure S3. Plots of the difference (denoted by $c - c_{CM}$) between the abscissas of c and c_{CM} along the segment $[c_1, c_2]$ as a function of $a_2 = 1 - a_1$, for different values of the spots' widths $\sigma_1 \approx \sigma_2$, and assuming $|c_1 - c_2| = 1$. Note that $c - c_{CM}$ is < 0 or >0 according as $a_2 < 0.5$ or $a_2 > 0.5$; in other words, the one-center position tends to lie closer to the brighter spot than does the CM.

S4. Positional correlations and MSD of a Brownian particle in a central harmonic potential

a) Brownian particle in a harmonic potential without drift

Consider the motion of a particle constrained to two dimensions and subject to random forces originating from thermal fluctuations in the surrounding medium, to which add a non-random, frictionless restoring force $F_{\rm el}(x) = -\nabla V(x)$ reflecting the anchoring of the particle to some elastic structure. Here $x = (u, v)$ denotes the particle's position in the plane where it moves, which we also write $x = u + iv$, adopting complex notations.

The equation of motion of such a particle is given by the overdamped Langevin equation, which takes the form

$$\eta \frac{dx}{dt} + \nabla V(x) = f(t) \tag{6}$$

Here η is the friction coefficient of the particle and $f(t) = (f_x(t), f_y(t)) = f_x(t) + i f_y(t)$ is a fluctuating force vector resulting from the numerous collisions of the particle with the surrounding molecules of the medium (of the order of 10^{12} per second)(3). For a particle the size of a centrosome ($\sim 0.2\mu$m) immersed in aqueous solution, the above equation provides a valid description of the particle motion over timescales longer than a few ms. For shorter timescales inertia effects ignored by the above equation need to be taken into account. At experimentally relevant timescales (which may reach the millisecond but are always much slower than molecular timescales), the force $f(t)$ behaves like a Gaussian white noise, i.e. a stochastic process having a centered gaussian distribution at any given time, and whose values at different times are uncorrelated. Such a process is characterized by its first and second moments,

$$\langle f(t)\rangle = 0, \quad \langle f(t)f(t')^*\rangle = C\delta(t-t') \tag{7}$$

where $\delta(t-t')$ is Dirac's delta and C is a positive constant that sets the intensity with which the particle is bombarded by the surrounding molecules at thermal equilibrium. As C is ultimately determined by the equipartition theorem, it depends on the medium's temperature T as well as on particle characteristics that determine the diffusion coefficient D and the friction coefficient η (see below).

We will restrict our attention to the case of a central-symmetric harmonic potential $V(x) = V_0|x|^2$, for which simple analytic expressions for the correlation functions and the MSD can be derived. The restoring force then obeys Hooke's law $F_{\text{el}}(x) = -kx$ (with a spring constant $k = 2V_0$), and the Langevin equation becomes

$$\eta\frac{dx}{dt} + kx = f(t), \tag{8}$$

for which the solution with initial condition $x(0) = x_0$ reads

$$x(t) = x_0 e^{-t/\tau_0} + \frac{1}{\eta}\int_0^t e^{-(t-t')/\tau_0} f(t')dt' \tag{9}$$

where $\tau_0 = \frac{\eta}{k}$ is the relaxation time of the particle. From this solution one obtains, taking averages : $\langle x(t)\rangle = \langle x_0\rangle e^{-t/\tau_0}$. Thus, for any sensible distribution of the initial position x_0, the average position of the particle rapidly regresses to 0 with time. After a time not much larger than τ_0, the particle reaches a stationary regime in which it continues to oscillate randomly around its equilibrium position but does not move on average.

We now compute the positional correlation function of the particle, defined by $C_x(\tau, t) = \langle x(t)x(t+\tau)^*\rangle - \langle x(t)\rangle\langle x(t+\tau)\rangle^*$. Using the above solution and a short computation, we find :

$$\begin{aligned}
&\langle x(t_1)x(t_2)^*\rangle \\
&= \langle (x_0 e^{-t_1/\tau_0} + \tfrac{1}{\eta}\textstyle\int_0^{t_1} e^{-(t_1-s_1)/\tau_0} f(s_1)ds_1)(x_0 e^{-t_2/\tau_0} + \tfrac{1}{\eta}\int_0^{t_2} e^{-(t_2-s_2)/\tau_0} f(s_2)ds_2)^*\rangle \\
&= \langle |x_0|^2\rangle e^{-(t_1+t_2)/\tau_0} + \tfrac{C}{\eta^2}\textstyle\int_0^{t_1} ds_1 \int_0^{t_2} ds_2 e^{-(t_1+t_2-s_1-s_2)/\tau_0}\delta(s_1-s_2) \\
&= \big(\langle |x_0|^2\rangle - \tfrac{C\tau_0}{2\eta^2}\big)e^{-(t_1+t_2)/\tau_0} + \tfrac{C\tau_0}{2\eta^2}e^{-|t_1-t_2|/\tau_0},
\end{aligned}$$

so that

$$C_x(\tau, t) = \frac{C\tau_0}{2\eta^2}e^{-|\tau|/\tau_0} + \big(\langle |x_0|^2\rangle - |\langle x_0\rangle|^2 - \frac{C\tau_0}{2\eta^2}\big)e^{-(2t+\tau)/\tau_0}. \tag{10}$$

To determine the constant C, note that if the particle starts at the origin, $x_0 = 0$, then in the limit $k \to 0$ (unconstrained particle) one should recover the correlation function of the standard 2-dimensional Brownian motion, given by $\langle x(t_1)x(t_2)^*\rangle = 4D\min(t_1, t_2)$, where D is the particle's diffusion coefficient. But in that limit we have (since $\tau_0 \to +\infty$)

$$\langle x(t_1)x(t_2)^*\rangle = \frac{C\tau_0}{2\eta^2}(1 - \frac{|t_1-t_2|}{\tau_0} - 1 + \frac{t_1+t_2}{\tau_0} + O(\frac{1}{\tau_0^2})) \to \frac{C}{\eta^2}\min(t_1, t_2). \tag{11}$$

Thus, we have $C = 4D\eta^2$, and from Einstein's relation $D = k_B T/\eta$ we also get $C = 4\eta k_B T$.

In the stationary regime $t \gg \tau_0$, $C_x(\tau, t)$ becomes independent of t. Up to exponentially small terms, we get $\langle x(t)\rangle = 0$ and

$$C_x(\tau) = \langle x(t)x(t+\tau)^* \rangle = \frac{C\tau_0}{2\eta^2} e^{-|\tau|/\tau_0} = 2D\tau_0 e^{-|\tau|/\tau_0}. \quad (12)$$

A formula for the MSD travelled by the particle as a function of time in the stationary regime is easily obtained from the last equation. Indeed, in this regime,

$$MSD(\tau) = \langle |x(t+\tau) - x(t)|^2 \rangle = \langle |x(t+\tau)|^2 \rangle + \langle |x(t)|^2 \rangle - 2\mathrm{Re}\langle x(t+\tau)x(t)^* \rangle$$

$$= 4D\tau_0(1 - e^{-|\tau|/\tau_0}). \quad (13)$$

Thus, after a brief period of linear growth, the MSD curve saturates to a constant value $A = 4D\tau_0$ proportional to the area of the region in which the particle is confined. This saturation occurs on a timescale of the order of the relaxation time τ_0. The last two statements remain qualitatively true for confinement potentials that are not harmonic. In fact, Eq. 13 with $4D\tau_0$ replaced by an arbitrary parameter A provides a good empirical model for the MSD curve in such cases (4).

b) Brownian particle in a harmonic potential subject to drift

Consider now the case of a Brownian particle constrained by a central harmonic potential well that is not static but subject to a slow (possibly random) drift. One can imagine that the particle is anchored to some elastic structure itself moving with time. It is then subject to a restoring force of the form $F_{\mathrm{el}}(x,t) = -k(x - x_0(t))$, where the centre position $x_0(t)$ is a function of t. Writing $x(t) = \tilde{x}(t) + x_0(t)$, we see that $\tilde{x}(t)$ satisfies the modified Langevin equation :

$$\eta \frac{d\tilde{x}}{dt} + k\tilde{x} = f(t) - \eta \frac{dx_0}{dt}. \quad (14)$$

We will assume that the drift is much slower than the thermally-driven motion of the particle, so that at any given time $|\frac{dx_0}{dt}| \ll |\frac{dx}{dt}|$. Then, neglecting the term $\eta \frac{dx_0}{dt}$, the equation for $\tilde{x}(t)$ reduces to the original Langevin equation for a particle in a harmonic potential centered at the origin, whose correlation functions are known. This approximation amounts to neglecting the friction experienced by the particle due to the motion of the potential in the bath. Mathematically, it corresponds to neglecting correlations between $\tilde{x}(t)$ and $x_0(t)$. The positional correlation function of the particle then decomposes into a "particle part" and a "drift part", namely

$$C_x(\tau,t) = \langle (\tilde{x}(t) + x_0(t))(\tilde{x}(t+\tau) + x_0(t+\tau)^* \rangle - \langle \tilde{x}(t) + x_0(t) \rangle \langle \tilde{x}(t+\tau) + x_0(t+\tau) \rangle^*$$
$$= \langle (\tilde{x}(t)\tilde{x}(t+\tau)^* \rangle - \langle \tilde{x}(t) \rangle \langle \tilde{x}(t+\tau) \rangle^* + \langle x_0(t)x_0(t+\tau)^* \rangle - \langle x_0(t) \rangle \langle x_0(t+\tau) \rangle^*$$

$$= C_{\tilde{x}}(\tau,t) + C_{x_0}(\tau,t). \quad (15)$$

Similarly, for the particle's MSD, we have

$$MSD(\tau) \approx \langle |\tilde{x}(t+\tau) - \tilde{x}(t)|^2 \rangle + \langle |x_0(t+\tau) - x_0(t)|^2 \rangle = MSD_{\tilde{x}}(t) + MSD_{x_0}(t),$$

up to terms that relax exponentially fast with a characteristic time τ_0. Let us consider two cases of experimental interest.

i) Non-random drift of constant slow velocity $x_0(t) = u_0 t$ ($u_0^2 \ll 4D/\tau_0$). In that case we have $C_{x_0}(\tau, t) = 0$: a constant drift has no effect on the correlation function $C_x(\tau, t)$. However, it affects the MSD, as we have

$$MSD(\tau) = \langle |\tilde{x}(t+\tau) - \tilde{x}(t)|^2 \rangle + u_0^2 \tau^2 = 4D\tau_0(1 - e^{-|\tau|/\tau_0}) + u_0^2\tau^2 \tag{16}$$

ii) Slow Brownian drift with diffusion coefficient D_0 ($D_0 \ll D$) starting at the origin. In that case we have $\langle x_0(t) \rangle = 0$, and $C_{x_0}(\tau, t) = \langle x_0(t) x_0(t+\tau)^* \rangle = 4D_0 t$ ($\tau > 0$), so that for $t \gg \tau_0$ we get

$$C_x(\tau, t) = 2D\tau_0 e^{-|\tau|/\tau_0} + 4D_0 t. \tag{17}$$

Hence the positional correlation function is no longer stationary but displays slow linear growth for $t \gg \tau_0$. Similarly, for the MSD we get (again for $t \gg \tau_0$)

$$MSD(\tau) = \langle |\tilde{x}(t+\tau) - \tilde{x}(t)|^2 \rangle + \langle |x_0(t+\tau) - x_0(t)|^2 \rangle = 4D\tau_0(1 - e^{-|\tau|/\tau_0}) + 4D_0\tau \tag{18}$$

As a consequence of the above formulae, the correction to the zero-drift situation for the MSD is quadratic in the first case, and linear in the second. This results in easily distinguishable shapes of the MSD curve at short times, for which MSD measurements are most precise.

Supporting References

1. Boutet de Monvel, J., S. Le Calvez, and M. Ulfendahl. 2001. Image restoration for confocal microscopy : improving the limits of deconvolution, with application to the visualization of the mammalian hearing organ. Biophys. J. 80 : 2455–2470.
2. Jin, S., P.M. Haggie, and A.S. Verkman. 2007. Single-particle tracking of membrane protein diffusion in a potential : simulation, detection, and application to confined diffusion of CFTR Cl- channels. Biophys. J. 93 : 1079–1088.
3. Risken, H. 1996. The Fokker-Planck Equation : Methods of Solutions and Applications. Springer.
4. Destainville, N., A. Saulière, and L. Salomé. 2008. Comment to the article by Michael J. Saxton : A biological interpretation of transient anomalous subdiffusion. I. qualitative model. Biophys. J. 95 : 3117–3119 ; author reply 3120–3122.